Ignition Delay Time Measurements of Diesel and Gasoline Blends

Mohammed Alabbad[*1], Yang Li[1,2], Khalid AlJohani[1], Gavin Kenny[2], Khaiyom Hakimov[1], Moaz Al-lehaibi[1], Abdul-Hamid Emwas[1], Patrick Meier[2], Jihad Badra[3], Henry Curran[2], Aamir Farooq*[1]*

[1]*King Abdullah University of Science and Technology (KAUST), Clean Combustion Research Center, Physical Sciences and Engineering Division, Thuwal 23955-6900, Saudi Arabia*
[2]*National University of Ireland, Galway (NUI Galway), Galway, Ireland*
[3]*Transport Technologies Division, R&DC, Saudi Aramco, Dhahran, Saudi Arabia*
[*]Corresponding authors emails: mohammed.abbad@kaust.edu.sa; aamir.farooq@kaust.edu.sa

Abstract

Blends of diesel and gasoline can be used to achieve certain desired ignition characteristics in advanced compression ignition engine concepts. In this work, ignition delay times were measured for two blends of diesel and gasoline in two shock tubes and in a rapid compression machine. These blends comprised of 50/50 and 75/25 volumetric % of gasoline and diesel. To ensure complete vaporization of the blends, the prepared samples were analyzed with nuclear magnetic resonance (NMR) and laser absorption. The analyses revealed full evaporation, and negligible decomposition/oxidation occurred during mixture preparation. Ignition delay measurements covered wide ranges of temperatures (710 – 1349 K), pressures (10 and 20 bar), and equivalence ratios (0.5, 1.0 and 2.0). The measured ignition delay times of the two dieseline blends are compared with experimental data of low- to mid-octane gasoline, and low- to high-cetane fuels. The measured data are also compared with the simulated ignition delay times of primary reference fuel (PRF) and toluene primary reference fuels (TPRF) surrogates. Multi-component surrogates are proposed for the dieseline blends, and the measured ignition delays of multi-component surrogates and dieseline blends are in very good agreement.

Keywords: Dieseline, Diesel, Gasoline, Shock tube, Rapid compression machine, Ignition delay time, Surrogate.

1. Introduction

Energy is essential for the economic growth and sustainability of our society. Increasing population and rising standard of living will require even more energy in the future. For the transportation sector, liquid petroleum-derived fuels and internal combustion engines continue to dominate the market [1] but are one of the main sources of greenhouse gas emissions. Global warming which is a result of increasing greenhouse gas emissions is a critical environmental challenge. Likewise, harmful emissions from combustion, such as NOx and soot particles, directly affect human health. Currently the US and Europe aim to derive fuels from biomass, and shift towards hybrid and electric vehicles, and fuel-cell systems. However, the high energy density of hydrocarbon fuels is not matched by most alternative energy resources. Therefore, as we gradually transition to cleaner sources of energy, it remains imperative to improve the efficiency and reduce the emissions of internal combustion engines (ICEs).

Today, conventional gasoline and diesel engines are the primary engines in the light-duty vehicles market. The efficiency and emission concerns of these engines motivate a search for advanced combustion engine technologies. Various advanced combustion engine designs have been studied to overcome the low efficiency of gasoline engines and the high emissions of diesel engines. These advanced combustion strategies include homogeneous charge compression ignition (HCCI), premixed charge compression ignition (PCCI), reactivity-controlled compression ignition (RCCI) and partially premixed combustion (PPC). Advanced low-temperature combustion strategies can yield low NOx, low soot emissions and high efficiency.

The premixed compression ignition (PCI) combustion mode may be used to decrease soot and NOx emissions, and simultaneously increase efficiency [2-11]. Recent studies propose PCI engines to be powered by mid-octane gasoline fuels with research octane number (RON) ranging between 70 and 85 [6-9]. Today, at gas filling stations, there are either high-octane gasoline fuels or high-cetane diesel. Providing a mid-octane fuel to the customers would require significant modifications in the infrastructure of crude oil refineries and filling stations. To overcome this challenge, one potential route is to blend high-octane gasoline with high-cetane diesel to meet the fuel reactivity needed for advanced compression engine.

Many studies have shown that the use of gasoline and diesel blends, known as dieseline, in PPCI and HCCI engines can maintain combustion stability and decrease soot and NOx emission [4, 12-19]. Dieseline blends can enhance PCI combustion at low-to-medium loads [3, 4, 12, 20-

23]. These blends may also help extend the low misfire limit, increase engine stability, reduce peak cylinder pressures and reduce emissions within the entire HCCI operating window [12]. In addition to fuel injection timing, longer ignition delays may be achieved by increasing the gasoline ratio in the blend [24]. It has also been shown that dieseline blends may provide better fuel economy performance compared with pure diesel under advanced combustion modes [25]. Furthermore, blending diesel with gasoline can improve the spray atomization process [26].

IDTs of gasoline fuels have been measured in literature using shock tubes and rapid compression machines. In general, gasoline fuels are found to have similar reactivity at high temperatures. In the NTC region, the reactivity of gasoline fuels exhibits strong dependence on octane numbers and composition. [27-29]. At low temperatures, gasoline fuels show weaker dependence on octane numbers and composition [29]. Comparing gasoline fuels with simple surrogates such as PRF and TPRF revealed that matching the octane number can be sufficient to mimic the fuel reactivity at high temperatures and NTC regime [27, 28, 30, 31]. At low temperatures, matching the octane numbers is not sufficient to replicate the reactivity of the fuels, particularly for gasoline fuels with high octane sensitivity and high aromatic content. For such fuels, more complex surrogates that match other fuel properties (e.g., C/H ratio, density, and composition) may be needed [28, 30-32].

Several IDT studies have been conducted for fuels with high average molecular weight (relative to gasoline), such as diesel and jet fuel. Similar to gasoline fuels, diesel fuels, in general, have similar reactivity at high temperatures [33-38]. However, some slight effects of the degree of branching and cetane number on ignition delays may exist, where fuels with higher cetane number may have slightly higher reactivity [39, 40]. However, another study showed that fuels with widely varing cetane numbers exhibited similar reactivity at high temperatures [41]. In the NTC region, diesel fuels with similar cetane numbers have similar reactivity [35, 38, 41, 42]. At low temperatures, the reactivity of diesel fuels may depend on cetane number as well as moelcular composition [35].

There has been only one previous study on the IDTs measurements of gas phase dieseline (gasoline/diesel) blends. Wang et al. [43] measured IDTs of three dieseline blends (diesel proportions of 30%, 50%, and 70% by volume) in a shock tube and RCM. They covered temperature range of 636 – 1317 K, pressures of 6, 10 and 20 bar, and equivalence ratios of 0.5, 1.0 and 1.5. They proposed multi-component surrogates and compared the prediction of the

surrogates' models with the measured IDTs of the three blends. In a separate work, Wang et al. [44] measured IDTs of the three surrogates proposed previously and compare them with the predictions of the surrogate models.

IDT studies of jet fuels and diesels are listed in Table 1. For a summary of IDTs of gasoline fuels, the reader is referred to Sarathy et al. [29].

Table 1. Literature IDT studies of jet fuels, diesel and dieseline.

Year	Authors	Fuel	Diluent	Reactor	Temperature	Pressure	ϕ	CN / ON
2008	Vasu et al. [33]	Jet-A, JP-8	Air	ST	715 – 1229 K	17 – 51 atm	0.5 and 1.0	CN (JP-8) = 43.3
2009	Haylett et al. [45]	DF-2	Ar	AST	900 – 1300 K	2.3 – 8 atm	0.3 – 1.35	
2010	Kumar and Sung [46]	Jet-A, JP-8	Air/ Ar	RCM	650 – 1100 K	7, 15 and 30 bar	0.42 – 2.26	
2012	Haylett et al. [40]	Diesel-US	Ar	ST	838 – 1381 K	1.71 – 8.63 atm	1 – 2	CN = 43
		Diesel-Euro						CN = 55
		Diesel - Belarus						
2014	Gowdagiri et al. [41]	F-76	Air	ST	671 – 1266 K	10 & 20 atm	0.5 & 1.0	DCN = 48.8
		HRD-76						DCN = 78.5
2015	Hoang and Thi [47]	Palm oil / diesel blends	Air	ST	1174 – 1685 K	0.12 MPa	0.5, 1.0, 1.5	
		Palm oil (biodiesel)						CN = 37.39
		diesel						CN = 49
2016	Kukkadapu and Sung [48]	ULSD#2	N2, Fuel 0.514% fixed	RCM	678 – 938 K	10, 15 & 20 bar	0.5, 0.69 & 1.02	CN = 43.3, DCN = 43.7
		FD9A						CN = 43.9, DCN = 44.2
2016	Davidson et al. [36]	Jet-A1, -A2 and -A3	Air	ST	700 – 1250 K	12 atm	1.0	

2017	Flora et al. [34]		Ar	ST	980 – 1800 K	16 atm	0.5	
2017	Valco et al. [35]	Jet-A1	Air	RCM - DTC	625 – 735 K	30 bar	0.25, 0.5 & 1.0	CN = 40.4
		Jet-A2						CN = 47
		Jet-A3						CN = 47.9
		Jet-C1						CN = 17.1
		Jet-C2						CN = 50.4
		Jet-C3						CN = 47
		Jet-C4						CN = 28
		Jet-C5						CN = 39.6
2017	Davidson et al. [37]	JP-8 (A1); Jet-A (A2); JP-5 (A3); RP-2 (R4); RP-2 (R5); Kerosene (K6); Kerosene (K7); DF-2 (D8); DF-2 (D9); G10	Air/ Ar	ST	1000 – 1400 K	6 – 60 atm	1.0	
2018	Burden et al. [49]	Jet A1	Air	ST	660 – 1310 K	1, 2.14 & 4 MPa	1.0	DCN = 48.8
		Jet A2						DCN = 48.3
		Jet A3						DCN = 39.2
		Jet A; S-8; Sasol IPK; JP-5; HRJ-5; F-76; HRD-76						DCN available in the paper

2019	Yu et al. [42]	Diesel China Stage_V	Air	RCM	687 – 865 K	10 – 20 bar	0.37 – 1.25	CN = 52.5, DCN = 54.9
		Diesel China Stage_VI						CN = 52, DCN = 52.8
2019	Alturaifi et al. [38]	Jet-A	Air	ST	785 – 1293 K	7 – 26 atm	0.5 and 1.0	
		RP-1						
		DF-2						
2019	Mao	RP-3	air	ST/ RCM	625 – 1437 K	10, 15 & 20 bar	0.5 – 1.5	CN = 43.3
2019	Yu et al. [50]	China,s stage 6 diesel	Air	RCM	685 – 865 K	10, 15 & 20 bar	0.37 – 1.0	CN = 52
2019	Wang et al. [39]	A2; A4; A5; A6; A7; A8; CN30; CN35; CN40; CN45; CN50; CN55	Ar		1250 – 1450 K	4 atm	1.0	DCN available in the paper
2017	Javed et al. [51]	LN	Air	ST/ RCM	640 – 1250 K	20 & 40 bar	0.5, 1.0 & 2.0	RON = 64.5, MON = 63.5
2018	Alabbad et al. [30]	HSRN	Air	ST	620 – 1223 K	20 & 60 bar	0.5, 1.0 & 2.0	RON = 60, MON =58.3
2019	AlAbbad et al. [31]	GCI blend	Air	ST/RCM	640 – 1175 K	20 & 40 bar	0.5, 1.0 & 2.0	RON = 77 MON = 73.9
2019	Wang et al. [43]	Dieseline 30, 50 and 70	Air	ST/ RCM	636 – 1317 K	6 – 20 bar	0.5 – 1.5	

To assess the feasibility of using dieseline as a potential fuel for advanced compression ignition engines, we need to understand their reactivity trends in fundamental experiments to propose suitable surrogates and predictive chemistry models. In this work, two blends of diesel and gasoline fuels have been studied in a shock tube and an RCM. The formulated blends (dieseline blends) have diesel/gasoline volumetric ratios of 50/50 and 25/75, and have research octane numbers (RON) of 61 and 80, respectively.

2. Experimental Methodology

IDTs of two dieseline blends were measured in two high-pressure shock tubes (HPSTs) at King Abdullah University of Science and Technology (KAUST) and National University of Ireland, Galway (NUIG), and a rapid compression machine (RCM) at NUIG. The experiments cover temperature range between 710 and 1349 K, at two pressures (10 bar and 20 bar) and at three equivalence ratios (0.5, 1.0 and 2.0).

2.1. KAUST HPST Facility

The shock tube is constructed from stainless steel with an inner diameter of 10 cm. The driven section is 6.6 m long, and the driver section has a modular design to vary its length from 2.2 m to a maximum of 6.6 m. In this study, 2.2 m driver was used. The mid-section of the shock tube houses two pre-scored aluminum diaphragms in a double diaphragm arrangement (DDA) which allows better control of the post-reflected shock conditions compared to single diaphragm arrangement (SDA). Sidewall pressure and electronically excited OH* chemiluminescence were monitored using a Kistler 603B1 PZT and a photomultiplier tube (PMT), respectively, at 10.48 mm from the endwall. A schematic of the shock tube end-section is shown in Fig. 1(a).

The incident shock speed was measured using six PCB 113B26 piezoelectric pressure transducers (PZTs) placed in the last 3.7 m of the driven section of the shock tube. Incident shock attenuation rates varied from 0.5 to 1%/m. Post-reflected shock conditions (p_5 and T_5) were calculated using shock jump relations and known thermodynamic parameters, with uncertainties of $< 1.5\%$. A gradual pressure increase behind reflected shock wave, dp_5/dt, of ~ 4.5%/ms was measured. Thermodynamic properties of the dieseline blends were calculated using linear-by-mole averaging of the NASA polynomial coefficients of the proposed thermal surrogate (Section 2.6). Details of the HPST and the experimental procedure are provided in our previous work [52]. Due

to the low vapor pressure of the dieseline blends, the shock tube and the mixing vessel were heated to 180 ^{o}C to provide sufficient fuel volatility and to avoid fuel condensation.

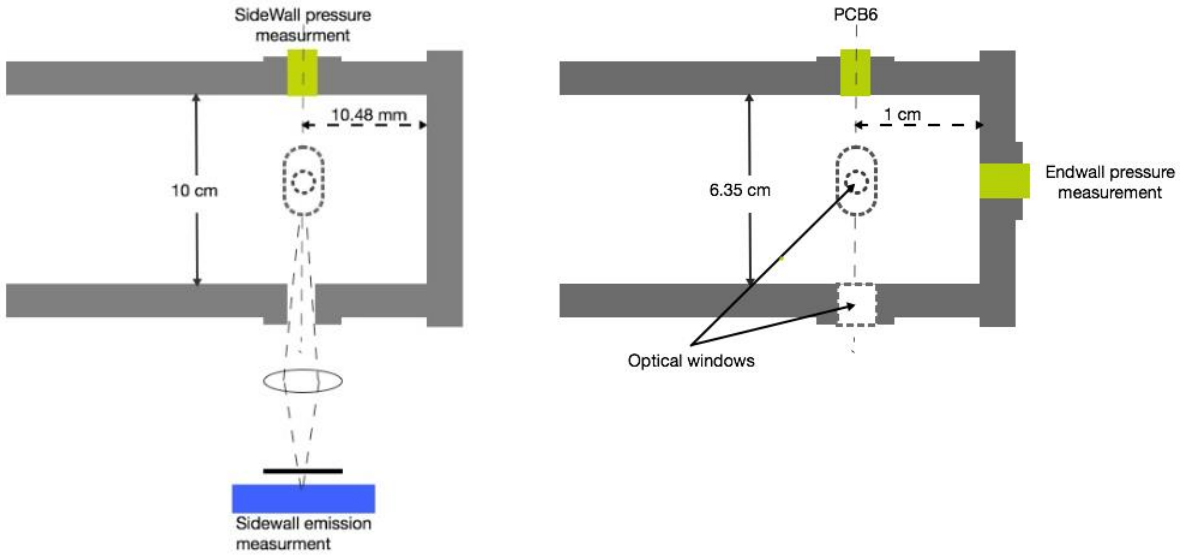

(a) (b)

Fig. 1. Schematic sketch of the HPST near endwall. (a) KAUST (b) NUIG.

2.2. NUIG HPST facility

The shock tube has a diameter of 6.35 cm. The driver and the driven sections have lengths of 3 m, and 5.73 m, respectively. The driver and the driven sections are separated by a 3 cm long double diaphragm housing. The pressure history at the endwall was recorded by a dynamic pressure transducer, from which the IDT was measured. The thermodynamic state of the test gas behind the reflected shock wave was evaluated from the ideal normal shock equations, which require the measurement of the shock velocity at the endwall. This measurement was performed by monitoring the incident shock arrival time at six pressure transducers staggered along the axis of the driven section and interpolating the velocity of the shock along the tube, and shock attenuation was accounted for by extrapolating the collective velocity measurements to the endwall. More detailed information about the shock tube can be found in reference [53]. A schematic of the shock tube end-section is shown in Fig. 1(b).

2.3. NUIG RCM Facility

The RCM has a 168 mm stroke and 38.2 mm bore. It has an opposed pistons configuration, which provides faster compression compared to single-piston machines. At the end of the stroke,

the pistons are locked which allows a constant volume reaction to proceed. The pressure-time history in the reaction chamber was recorded using a Kistler 603CAB pressure transducer.

The widely used adiabatic core model was employed to evaluate the compressed gas temperatures from pressure histories. Furthermore, the model was also used to prescribe energy release or heat loss. The compressed gas temperature (T_C) was calculated using isentropic relation from the initial temperature, initial pressure and measured compressed gas pressure (p_C). The uncertainty of the calculated T_C is conservatively estimated to be within ±10 K. More detailed information about the RCM can be found in reference [54].

2.4. Test Mixture Preparation and Fuel Evaporation

The fuel/air mixtures were prepared in mixing vessels. Due to the high molecular weight of the dieseline blends, the mixing vessels were heated to provide sufficient fuel volatility and avoid fuel condensation. In order to ensure homogenous mixture, the prepared mixtures were stored in the mixing vessels for a minimum of one and a half hour prior to the shock tube and RCM experiments (maximum time for the mixtures before being used is 4 hours). The mixing vessel and the shock tube at KAUST were heated up to 180 ^oC. The shock tube facilities at NUIG were heated up to 120 ^oC. The RCM facility was heated to 150 ^oC and the minimum initial temperature for RCM experiments was set to 150 ^oC. The total pressure for test mixtures for KAUST and NUIG mixing vessels did not exceed 4000 and 2000 Torr, respectively. Therefore, heating to 120 ^oC was sufficient for NUIG experiment while higher heating of 180 ^oC was need for KAUST experiments.

A molar ratio of 3.76:1 of N_2:O_2 was used to prepare fuel/air mixtures. The compositions of the test mixtures are available in Table 2. The molecular nitrogen and oxygen used to prepare the synthetic air were research grade (99.999%). The diesel and gasoline fuels used in the study are certified and supplied by Coryton. Properties of the individual fuels (gasoline, diesel) and the dieseline blends are listed in Table 3. Two dieseline blends were prepared. The first blend is 50% diesel and 50% gasoline by volume and named 50/50 dieseline. The second blend is 25% diesel and 75% gasoline by volume and named 25/75 dieseline. These blends were formulated to understand the reactivity enhancement induced by diesel addition to gasoline, and to study dieseline fuels with relatively low (61) and high (80) values of research octane number.

Table 2. Composition (in mole%) of test mixtures.

	50/50 Dieseline			25/75 Dieseline		
ϕ	0.5	1.0	2.0	0.5	1.0	2.0
Fuel	0.82	1.63	3.20	0.97	1.91	3.76
O_2	20.84	20.67	20.34	20.81	20.61	20.22
N_2	78.34	77.71	76.46	78.23	77.48	76.03

Table 3. Properties of the individual fuels and prepared dieseline blends.

Fuel	**Gasoline[1]**	**Diesel[1]**	**50/50 Dieseline**	**25/75 Dieseline**
RON	97.5	–	61	80
MON	86.6	–	55	73.8
Octane Sensitivity (OS)	10.9	–	6	6.2
DCN	17.3	56.7 (CN = 53.8)	39.0 (CN = 36)	28.3
H/C	1.776	1.8	1.78	1.78
Avg. molecular weight (g/mol)	90.6	179	122.5	104.6
Density @ 15 ºC (kg/L)	0.7485	0.83	0.8[2]	0.8[2]
Paraffins (Mol%)	10.1	38.1	20.2	14.5
Iso-paraffins (Mol%)	31.9	0.0	20.4	26.8
Naphthenes (Mol%)	5.0	29.6	13.9	8.9
Aromatics (Mol%)	33.6	22.3	29.5	31.8
Oxygenates (Mol%)	8.2	0	5.2	6.9
Olefins (Mol%)	11.2	0	7.2	9.4
Indane & tetralin (Mol%)	0.0	10.0	3.6	1.6
Average formula	$C_{6.46}H_{11.39}O_{0.1}$	$C_{12.97}H_{23.3}$	$C_{8.81}H_{15.69}O_{0.063}$	$C_{7.49}H_{13.28}O_{0.082}$

[1]Certified fuel supplied by Coryton. [2]Calculated using linear-by-mole relation.

At KAUST, samples of vaporized dieseline blends were taken from the shock tube and the mixing vessel for nuclear magnetic resonance (NMR) spectroscopy analysis to ensure proper evaporation of the fuels, to avoid condensation in the shock tube or the piping between the shock tube and mixing vessel, and to minimize fuel oxidation and decomposition during the mixing

waiting time. In order to determine the proper heating temperature, the mixing vessel and the shock tube were heated up to 6 different temperatures (150, 160, 170, 180, 190 and 200 ^{o}C) for sampling. Also, the samples were taken at different mixing waiting times of 1, 2, and 4 hours. The analysis showed signs of insufficient evaporation at heating temperatures below 170 ^{o}C. At 200 ^{o}C, the analysis showed change of fuel composition as a result of partial oxidation. Therefore, the shock tube and the mixing vessel were heated to 180 ^{o}C. Details about the NMR analyses are provided in Section 2.5.

In order to confirm the complete vaporization of the dieseline blends at NUIG, infrared (IR) absorption of 25/75 dieseline blend was measured in an optically accessible test cell and the HPST at a wavelength of 3.39 μm, following Beer-Lambert law:

$$A = \log\left(\frac{I_o}{I}\right) = \varepsilon c L$$

where ε is the molar absorption coefficient, A is the absorbance of light, L is the optical path length, I and I_0 are the transmitted and incident light intensities, respectively.

The absorption coefficient of the dieseline blend was measured in the test cell and found to be 9.62 m^2/mol. Absorption measurements for pure dieseline blend were conducted in the cell where complete evaporation can be observed. Later, absorption of stoichiometric mixtures of the dieseline blend were conducted in the heated shock tube to measure the blend concentration at the observation location near the endwall. Measurements in the shock tube covered the upper limit of the total pressure conducted in the experiments ($p_1 \approx 1500$ mbar). Figure 2 shows a good agreement between the measurements of pure dieseline blends in the test cell and the measurements of ϕ = 1.0 25/75 dieseline/air mixture in the HPST. Both the shock tube and the optical cell were heater to 120 ^{o}C.

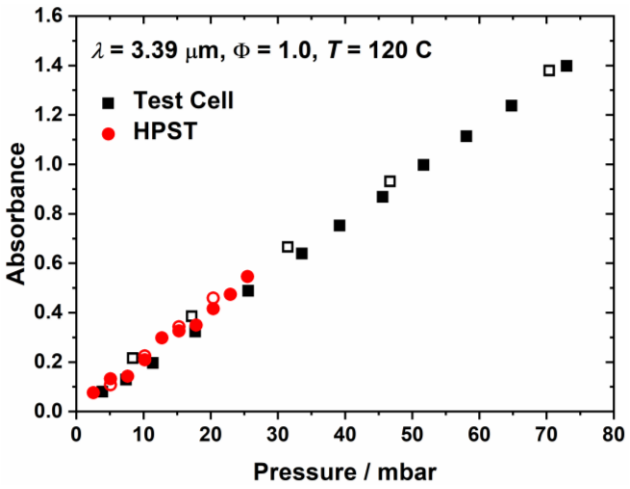

Fig. 2. Fuel concentration measurements by 3.39 μm He-Ne laser absorption. Measurements in the test cell were done with pure dieseline blend, whereas dieseline/air stoichiometric blend was used for in the HPST.

2.5. Nuclear Magnetic Resonance (NMR) Spectroscopy Analysis

Gas-phase IDT measurements of large hydrocarbons with low vapor pressures are challenging in shock tubes and RCMs. There are many shock tubes and RCM facilities equipped with heating elements to elevate the initial temperature for proper fuel evaporation. However, careful consideration should be given to heating temperature and temperature uniformity. The temperature should be uniform along the driven section as any non-uniformity in the temperature can lead to fuel condensation and bad shock quality. Detailed temperature measurements should be implemented to ensure cold spots are not formed at any part of the mixing vessel, piping and shock tube. Cold spots can lead to the condensation of the heavier components of the distillate fuel and thus change the composition of the fuel. At high preheating temperatures, for example, in the mixing vessels, large hydrocarbons may decompose or oxidize during the mixing waiting time. The mixing waiting time have been reported in literature to range from 1 hour to many hours to ensure mixture homogeneity. Longer mixing waiting times lead to a higher likelihood of fuel decomposition or oxidation. Therefore, as there is a minimum temperature to ensure full evaporation of fuels, there is a maximum temperature to avoid significant decomposition or oxidation.

In this work, shock tube and the RCM facilities were heated to ensure complete fuel evaporation. At NUIG laser absorption technique was used to ensure no fuel loss occurred due to insufficient evaporation or condensation. At KAUST, NMR analysis was conducted to ensure

complete fuel evaporation and minimal decomposition / oxidation. NMR analysis was carried out for 50/50 dieseline as it has more diesel concentration, i.e., larger fraction heavier hydrocarbons. To figure out suitable preheating temperature for the shock tube and the mixing vessel, the preheating temperature was varied between 150 to 200 ^{o}C (150, 160, 170, 180, 190 and 200 ^{o}C). Mixtures were prepared in the mixing vessels and kept for mixing for 2 and 4 hours. Samples were collected from the mixing vessel at various times. Samples were collected after half, one and two hours in order to investigate the minimum required mixing time to obtain homogenous mixture. Samples were collected after two and four hours to investigate the adequate preheating temperature and the maximum time for the mixture to be kept in the mixing vessel. For the samples collected from the shock tube, the mixtures were first prepared in the mixing vessel and kept for two hours mixing time; thereafter, the mixtures were released to the shock tube and samples were collected after 10 minutes. Dry-ice was used to trap the gaseous dieseline/air samples, and these were kept in a fridge before NMR testing to prevent the evaporation of light components.

A Bruker NMR spectrometer (700 MHz AVANACIII), equipped with CPTCI multinuclear CryoProbe, was used for NMR analysis. The samples were prepared by dissolving 70 μL of the samples in 600 μL of a deuterated chloroform $CDCl_3$ solvent in a 5 mm diameter NMR tube. To achieve a high signal-to-noise ratio, ^{1}H NMR spectra were recorded by collecting 64 scans with a recycle delay time of 10 s. Temperature for all the analyses was maintained at 298 K. Spectral signal of $CDCl_3$ at 7.24 ppm was used as a reference to determine the chemical shifts. Flame ionization detector (FID) signals were amplified by applying exponential line-broadening factor of 0.3 Hz prior to a Fourier transformation. Using NMR analysis, the composition of a fuel can be described in terms of the functional groups, such as paraffinic CH_3 groups, paraffinic CH_2 groups, paraffinic CH groups, olefinic $CH=CH_2$ groups, naphthenic $CH-CH_2$ groups, aromatic C-CH groups, and ethanolic OH groups. These functional groups can be accurately distinguished as they produce a distinct peak in the ^{1}H NMR spectra. The characteristic ^{1}H NMR structural assignments of the functional groups are presented in Table 4. More details about the ^{1}H NMR hydrocarbon characterization for conventional fuels can be found in reference [55].

The NMR analysis showed that a minimum of 170 ^{o}C preheating temperature is required to ensure complete evaporation of the dieseline fuel. However, preheating temperature of 190 ^{o}C or higher resulted in significant change of fuel composition. Figure 3 shows the NMR results of two of the samples taken from the mixing vessel at preheating temperature of 190 and 200 ^{o}C. It

is observed that the samples taken from the mixing vessel have new species (green and red line peaks at δ = 5.0 ppm), which do not exist in the pristine sample taken from the bottle (flat black line at 5.0 ppm).

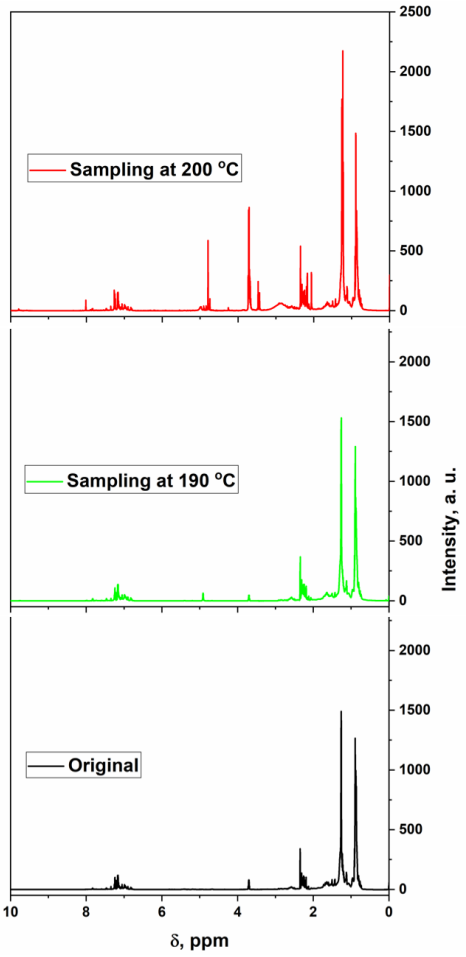

Fig. 3. NMR spectra for a 50/50 dieseline sample taken from the mixing vessel at 190 and 200 °C and compared with a pristine sample taken from the original dieseline bottle.

intensity	Region (ppm)	Significance
A	6.42–8.99	aromatics
B	4.50–6.42	olefinic CH and CH_2 groups
C	2.88–3.40	α-CH

D	2.64–2.88	α-CH_2
E	2.04–2.64	α-CH_3
F	1.57–1.96	naphthenic CH and CH_2 groups
G	1.39–1.57	paraffinic CH groups
H	0.94–1.39	paraffinic CH_2 groups
I	0.25–0.94	paraffinic CH_3 groups

Table 4. Regions of the proton ^{1}H NMR spectra for hydrocarbon analysis. [56-58]

Figure 4 shows the results of NMR analyses at different temperatures (150 – 200 ºC). At each temperature, the sampling and the analysis were repeated at least two times. The repeated sampling resulted in very similar results except for some samples at high temperatures of 190 and 200 ºC where significant changes in composition were observed. Figure 4 plots average of all the samples with precise results at the labelled temperature. Figure 4 shows that the samples taken at prehearing temperature of 180 ºC have better agreement with the original sample from the bottle. Therefore, for all experiments conducted in the KAUST HPST, the preheating temperature for the shock tube and mixing vessel was set to 180 ºC. To sample at 180 ºC, samples were analyzed at 3 different mixing waiting times of 1, 2 and 4 hours. The results showed that the test mixture can remain in the mixing vessel up to 4 hours with no significant decomposition or oxidation.

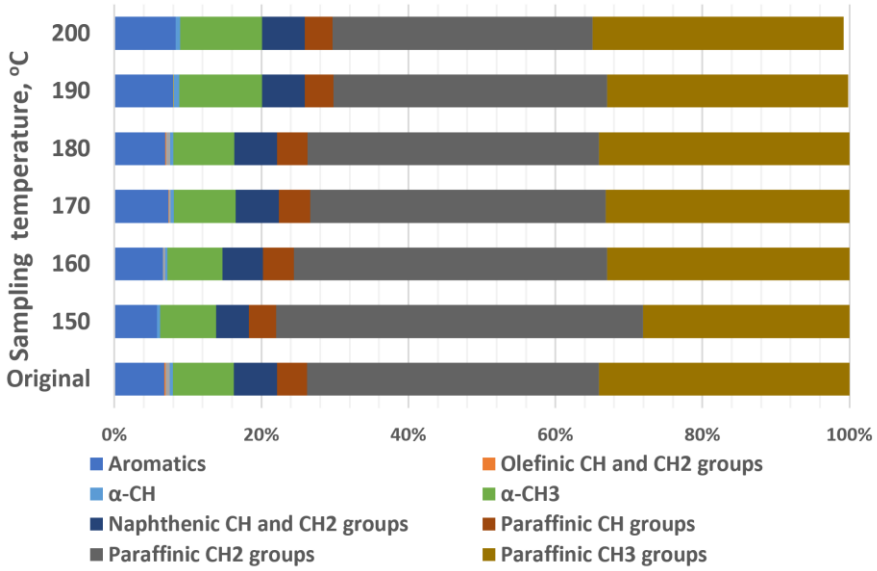

Fig. 4. NMR analyses results for samples taken from the bottle and mixing vessel at 6 preheating temperatures.

2.6. Surrogate Formulation

Three different surrogates are proposed in this work for each of the dieseline blend: (a) a two-component PRF surrogate to match the RON of the fuel, (b) a three-component TPRF surrogate to match the RON and MON of the fuel, (c) a multi-component surrogate (MCS) to match RON, MON, H/C ratio and fuel composition. The MCS for dieseline is formulated by combining the surrogates previously proposed by Lee et al. [32] for Coryton gasoline and by Jameel et al. [59] for Coryton diesel. The dieseline surrogate blend was prepared as per the molar ratio of diesel and gasoline in the dieseline blend. For example, the molar fraction of Coryton diesel and Coryton gasoline in the 50/50 dieseline blend is 36 mol% and 64 mol%, respectively, and therefore, its surrogate is a blend of 36 mol% diesel surrogate components and 64 mol% gasoline surrogate components. Compositions of the multi-component surrogates (MCSs) are provided in Table 5.

	Components	**25/75 Dieseline MCS**	**50/50 Dieseline MCS**
Coryton Gasoline	*n*-Butane	6.12	4.65
	2-Methyl butane	7.28	5.53
	Ethanol	7.86	5.97
	1-Hexene	10.49	7.96
	n-Heptane	2.62	1.99
	2,2,4-Trimethylpentane	17.35	13.17
	Toluene	28.83	21.90
	cyclohexane	3.62	2.75
Coryton Diesel	*n*-Hexadecane	3.98	9.06
	heptamethylnonane	2.88	6.55
	n-Butylcyclohexane	2.37	5.40
	n-Butylbenzene	6.61	15.05

Table 5. Composition (in mole%) of the multi-component surrogates for the two dieseline blends.

3. Results and Discussion

3.1. Ignition Delay Time Measurements

IDTs of the two dieseline blends (50/50 and 25/75 dieseline) and two multi-component surrogates (MCSs) were measured in two shock tubes and an RCM. Measurements were carried out at two pressures (10 and 20 bar), three equivalence ratios (ϕ = 0.5, 1.0 and 2.0), and a wide range of temperatures (710 – 1349 K). Experimental conditions are given in Table 6 and measured IDTs are tabulated in Table S1 (Supplementary materials). Detailed results and comparisons are provided in subsequent sections. In these sections, the effect of temperature, pressure, equivalence ratio and blending ratio are discussed. Also, comparisons with similar fuels are shown and discussed.

Table 6. Experimental conditions for ignition delay measurements.

	Pressure (bar)	Equivalent ratio	Temperature (K)
KAUST shock tube			
25/75 Dieseline	20	1.0	727 – 1093
50/50 Dieseline	10	1.0 and 2.0	710 – 1111
	20	0.5, 1.0 and 2.0	704 – 1229
25/75 MCS	20	1.0	729 – 1112
50/50 MCS	20	1.0	712 – 1131
NUIG shock tube			
25/75 Dieseline	10 and 20	0.5 and 1.0	910 – 1364
NUIG RCM			
25/75 Dieseline	10 and 20	0.5, 1.0 and 2.0	703 – 979
50/50 Dieseline	10 and 20	0.5	753 – 983

In the shock tube measurements an IDT is defined as the time between the arrival of the reflected shock wave and the onset of the ignition near the endwall. The arrival of the reflected shock wave was determined by step rise in pressure at the observation point. The onset of ignition was detected by the maximum slope in the sudden increase of pressure or OH* sidewall. IDT data presented in this work were mostly deduced from the pressure signal. Representative IDT

measurements are shown in Fig. 5. Uncertainty in the reported IDTs is estimated to be about 20%. This uncertainty primarily comes from the uncertainty in the calculated reflected shock temperature and mixture composition. The gradual pressure rise behind reflected shock wave, dp_5/dt, was measured to be approximately 4.5%/ms for KAUST and 4 %/ms for NUIG. This increase in pressure needs to be imposed for shock tube IDT simulations.

In the RCM measurements an IDT is defined as the time difference between end-of-compression (EOC) and the maximum rate of pressure rise due to ignition. IDTs were repeated three times for a single thermodynamic condition, and the reproducibility of the measured data was within 10% at similar compressed temperature and pressure. The overall uncertainty in RCM IDTs is estimated to be 15%. This uncertainty mainly comes from the uncertainty of T_c. The uncertainty of T_c is related to the measurement of initial pressure, temperature, compressed pressure (P_c), partial pressure of the mixture components and the thermodynamic data. A representative IDT measurement is shown in Fig. 6.

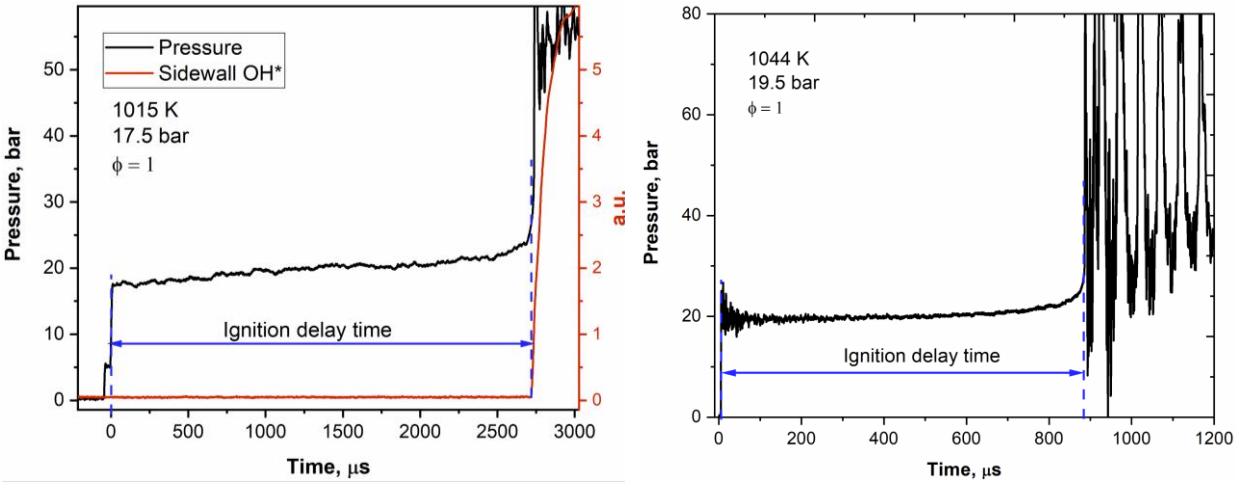

(a) (b)

Fig. 5. Representative IDT measurements; (a) 50/50 dieseline in the KAUST shock tube (b) 25/75 dieseline in the NUIG shock tube.

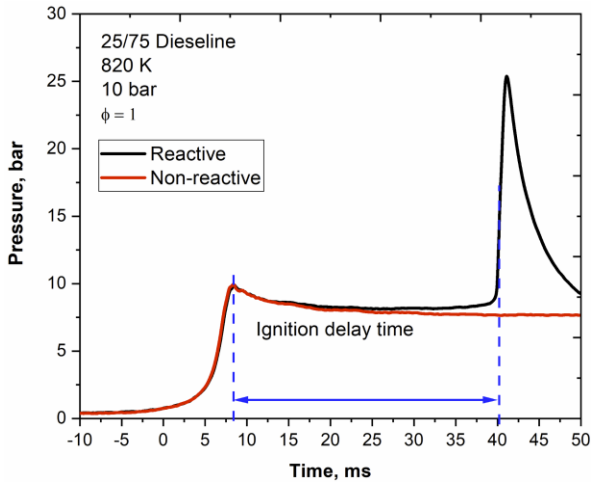

Fig. 6. Representative IDT measurement in the NUIG RCM.

3.2. Influence of Pressure on Ignition Delay Times

IDTs of the two dieseline blends were measured at two pressures (10 and 20 bar). Figure 7 shows the effect of pressure on ignition times at ϕ = 1.0. Experimental results show that the reactivity of the dieseline blends increases with increasing pressure. The effect of pressure is weak at high temperatures, and strong in the NTC regime. The chemistry of the reactions involving $\dot{O}H$, $H\dot{O}_2$ and H_2O_2 species plays important role in the NTC region. Two key reactions include the concerted elimination reactions of alkyl-peroxy ($R\dot{O}_2$) radicals to produce an olefin and $H\dot{O}_2$ radicals and hydroperoxy-alkyl ($\dot{Q}OOH$) radical propagation reactions. Hydroperoxy-alkyl radicals are more stable at low pressures and low temperatures. Therefore, the competition between chain branching and propagation reactions is driven by pressure and temperature. At intermediate temperatures, the overall reactivity is significantly affected by the pressure-dependent H_2O_2 decomposition reaction.

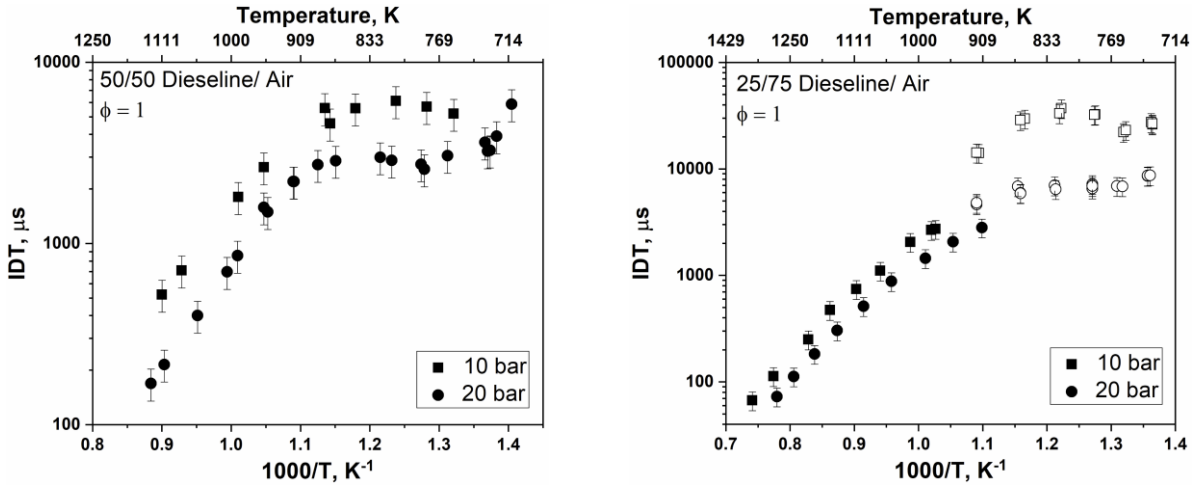

(a) (b)

Fig. 7. Influence of pressure on IDT. Shock tube: solid symbols. RCM: open symbols.

3.3. Influence of Equivalence Ratio on Ignition Delay Times

IDTs of the two dieseline blends were measured at three equivalence ratios (ϕ = 0.5, 1 and 2). Figure 8 shows influence of equivalence ratio on IDTs. Stronger influence of equivalence ratio is seen in the NTC region compared to high temperatures. The low-temperature chain branching pathway ($\dot{R} + O_2 \rightarrow R\dot{O}_2 \rightarrow \dot{Q}OOH + O_2 \xrightarrow{\text{Low temp.}} \dot{O}_2QOOH \rightarrow R\dot{O} + \dot{O}H + \dot{O}H$) is sensitive to the concentration of fuel radicals. This leads to overall higher reactivity for rich mixtures compared to lean mixtures at low temperatures. At higher temperatures, the overall reactivity is more sensitive to the decomposition of alkyl-peroxyl ($R\dot{O}_2$) radical and hydroxyl ($\dot{O}H$) radical chemistry. These pathways are less sensitive to fuel concentration, and, therefore, a lesser influence of equivalence ratio is seen at high temperatures.

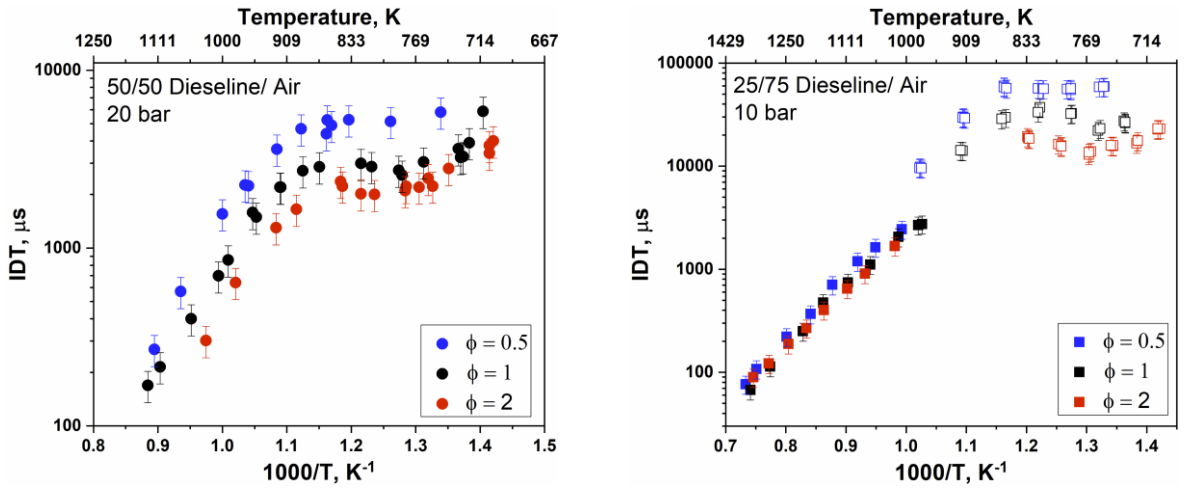

(a) (b)

Fig. 8. Influence of equivalence ratio on IDTs. Shock tube: solid symbols. RCM: open symbols.

3.4. Influence of Blending Ratio on Ignition Delay Time

Figure 9 presents a comparison between two blends of dieseline (50/50 and 25/75 dieseline) at ϕ = 1.0 and pressure of 20 bar for shock tube measurements. Results show that the blending effect on IDTs is weak at high and low temperatures. The 50/50 dieseline is slightly more reactive than the 25/75 dieseline at temperatures ~770 K ≥ T ≥ ~900 K. However, in the NTC region, the blending ratio does have an appreciable effect. Increasing the diesel ratio has strong effect increasing the reactivity of the dieseline blend at temperatures between ~ 770 K and ~900 K. Figure S1 (supplementary materials) shows the effect of blending ratio on IDTs at two pressures and three equivalence ratios covering high temperatures and NTC regime for both shock tube and RCM measurements. The figures show similar results as of Fig. 9, higher effect in the NTC region while weak effect at high temperatures. However, it shows also, higher effect of blending ratio at higher pressures and higher equivalence ratios.

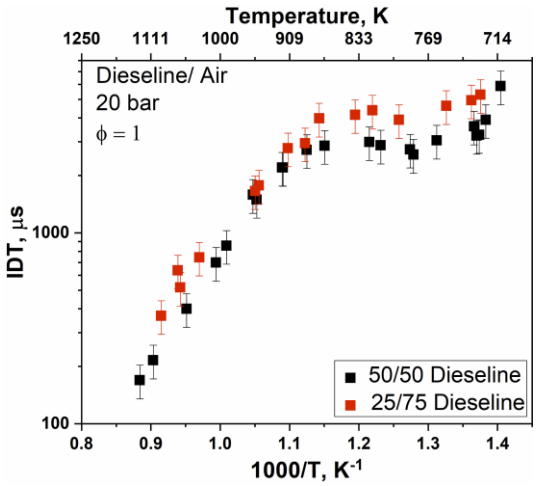

Fig. 9. Influence of diesel/ gasoline blending ratio on measured IDTs.

3.5. Comparison with Literature

3.5.1. Dieseline Fuels

In this section, our data are compared with IDT measurements of gas-phase dieseline by Wang et al. [43]. The diesel and gasoline used in Wang et al. [43] and this work have approximately similar octane/cetane numbers. However, Wang et al. [43] fuels have higher H/C ratios and higher average molecular formula. Fuel properties are compared in Table 7.

Fuel	Coryton Diesel This work	Coryton Gasoline This work	Diesel Wang et al. [43]	Gasoline Wang et al. [43]
RON	–	97.5	–	95
MON	–	86.6	–	87
OS	–	10.9	–	8
CN	53.8	–	52.8	–
H/C ratio	1.8	1.78	1.94	1.81
Average formula	$C_{12.97}H_{23.3}$	$C_{6.46}H_{11.39}O_{0.10}$	$C_{16.31}H_{31.65}$	$C_{7.21}H_{13.03}$

Table 7. Comparison between the diesel and gasoline used for the dieseline blends of this work and Wang et al. [43].

Figures 10 (a) and (b) shows that at high temperatures, the reactivity of the 50/50 dieseline blends of this work and Wang et al. arlee similar, especially at low pressures (10 bar) and low equivalence ratio (ϕ = 0.5). At higher pressure (20 bar) and higher equivalence ratio (ϕ = 1.0), slight difference in IDTs is noticed in the high-temperature region. In the NTC region, larger differences are seen between the 50/50 dieseline of Wang et al. [43] and this work, particularly at 20 bar for lean mixtures. Although gasoline and diesel fuels of this work and Wang et al. [43] have similar octane/cetane ratings, synergistic/antagonistic effects and compositional differences can cause reactivity differences between the two dieseline blends.

Figures 10 (c) and (d) shows a comparison between 25/75 dieseline blend of this work and 30/70 dieseline blend of Wang et al. [43]. Due to the higher fraction of diesel, the 30/70 dieseline is more reactive than the 25/75 dieseline at high temperatures and in the NTC region.

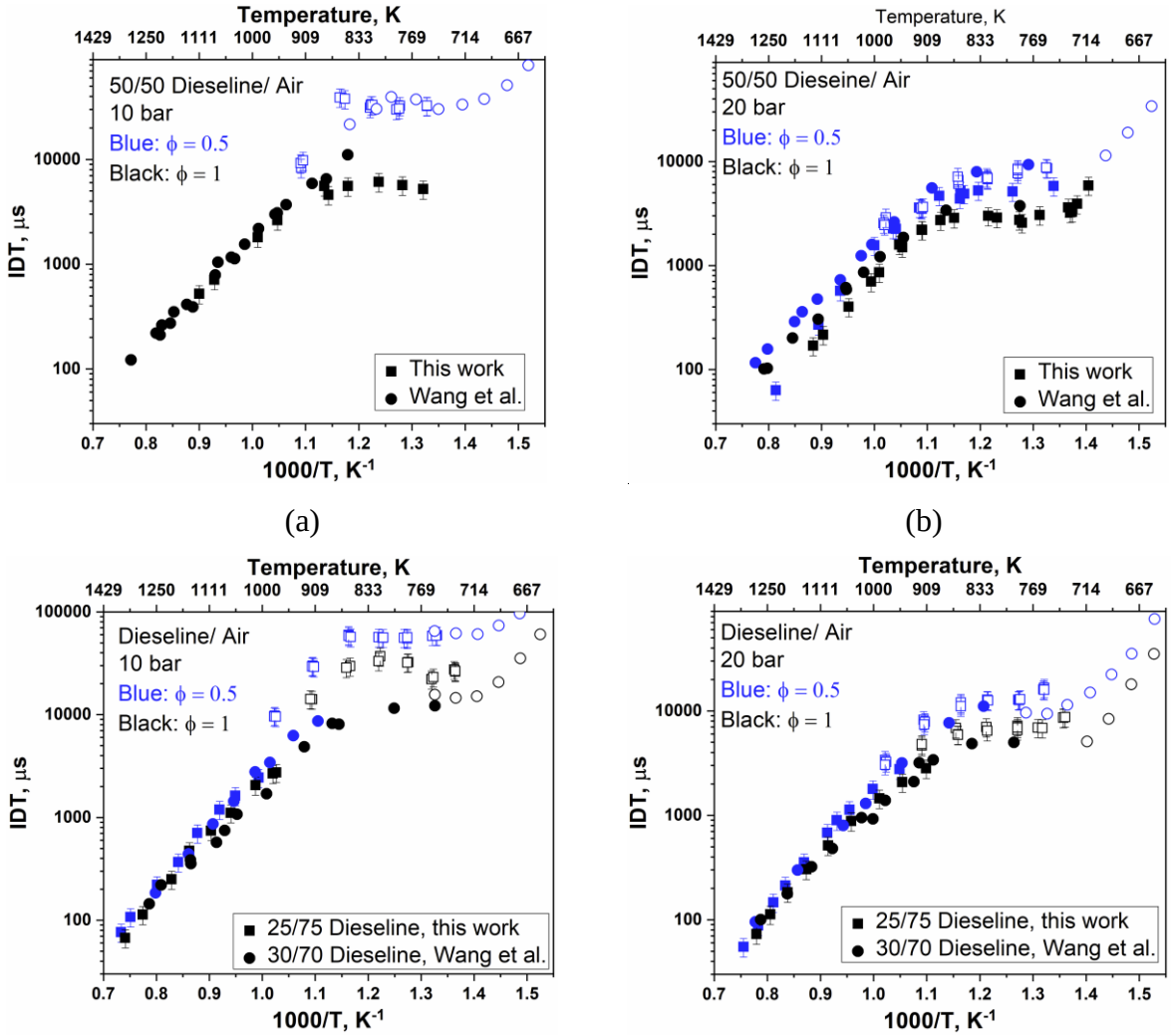

Fig. 10. Comparison between measured IDTs of Wang et al. [43] and this work. Solid symbols: shock tube. Open symbols: RCM.

3.5.2. Low Cetane Diesel and Low Octane Gasoline Fuels

Research octane number (RON) and DCN were measured for the 50/50 dieseline blend used in this work, and these values are 61 and 39.0, respectively. This makes it similar to a low-cetane diesel fuel or low-octane gasoline fuel. In Fig. 11(a), the 50/50 dieseline blend is compared with two low octane gasoline, a light naphtha (LN) ($C_{5.456}H_{15.69}$) [51] and a Haltermann straight run naphtha (HSRN, $C_{6.519}H_{13.997}$) [30], having RON of 64.5 and 60, respectively. Figure 11(a) shows that the dieseline blend has higher reactivity at high and low temperatures. In the NTC region, all three fuels expedite similar reactivity as they have approximately similar octane

numbers. More comparisons are shown in Fig. S2 (Supplementary materials). Figure 11(b) shows the composition of the three fuels. The 50/50 dieseline blend studied in this work has an average carbon number of 8.8, which is an indication of the presence of large hydrocarbons. These long-chain hydrocarbons can increase the reactivity of the fuel at high and low temperatures [60-62].

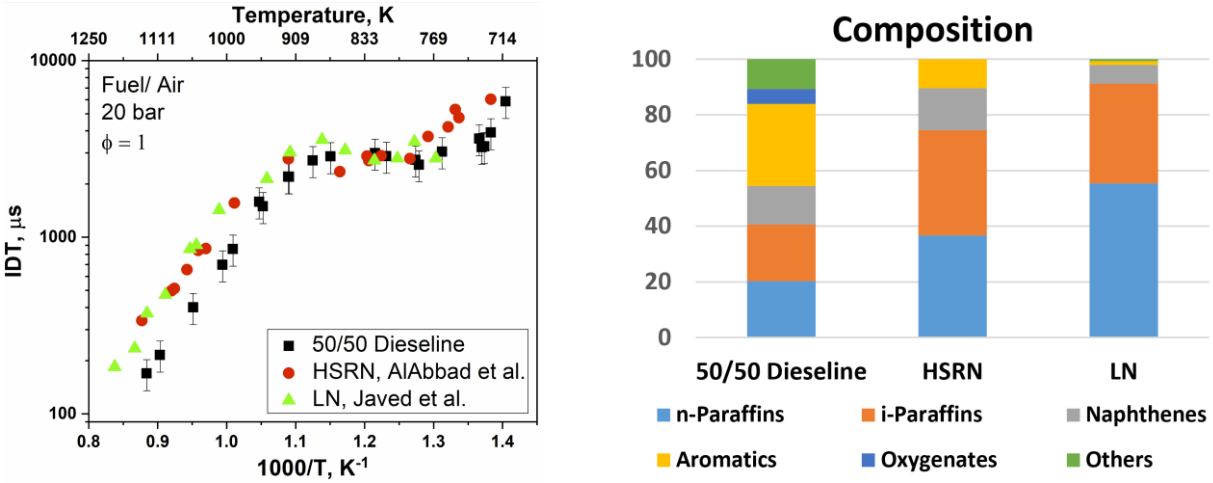

(a) (b)

Fig. 11. Comparison with low octane gasoline fuels. (a) Shock tube IDT measurements. (b) Fuels composition. 50/50 dieseline: this work, HSRN: AlAbbad et al. [30], LN: Javed et al. [51]. For dieseline, others include olefins, indanes and tetralines.

In Fig. 12, the 50/50 dieseline blend is compared with various jet fuels and diesel. The results show that all fuels have similar high-temperature IDTs with a relative standard deviation of 40%. The plotted fuels have cetane numbers distribution of CN/DCN = 36 – 48.8 (excluding HRD-76). In general, the comparison shows a weak effect of the cetane number on IDTs at high temperatures. However, the two diesel fuels, HRD-76 and F-76, exhibit shorter IDTs at 10 bar compared to other fuels. Figure 13 compares cetane number, H/C ratio, molecular weight and composition of the fuels plotted in Fig. 12. It may be argued that HRD-76 and F-76 having higher molecular weight exhibit shorter IDTs due to the presence of larger hydrocarbons. A comparison for lean mixtures at 20 bar is shown in Fig. S3 (supplementary materials).

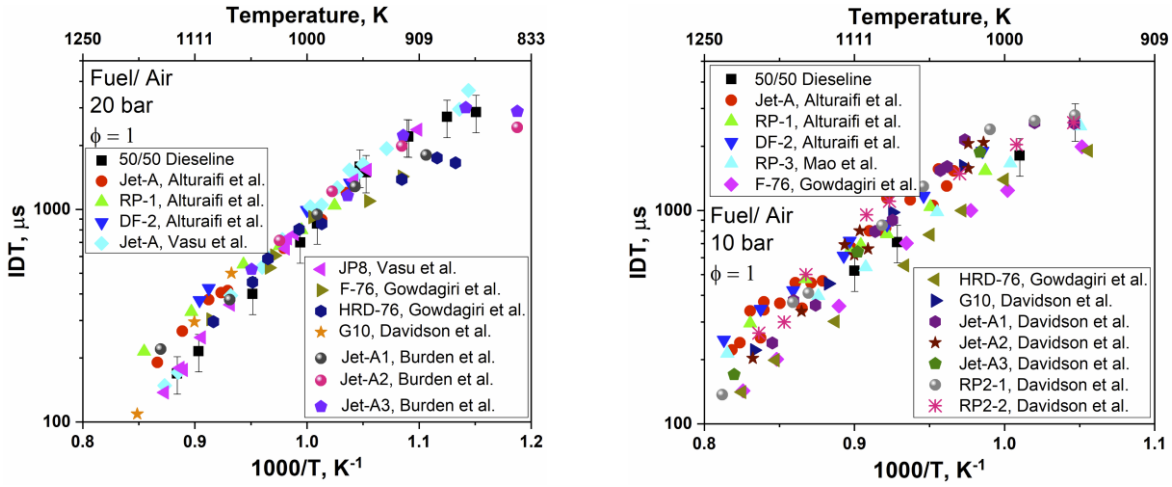

(a) (b)

Fig. 12. Comparison of 50/50 dieseline and various jet fuels / diesel. Jet-A, RP-1 and DF-2 by Alturaifi et al. [38]; Jet-A and JP8 by Vasu et al. [33]; F-76 and HRD-76 by Gowdagiri et al. [41]; G10 by Davidson et al. [37] ; Jet-A1, Jet-A2 and Jet-A3 by Burden et al. [41]; RP-3 by Mao et al. [63]; Jet-A1, Jet-A2, Jet-A3, RP2-1 and RP2-2 by Davidson et al. [36].

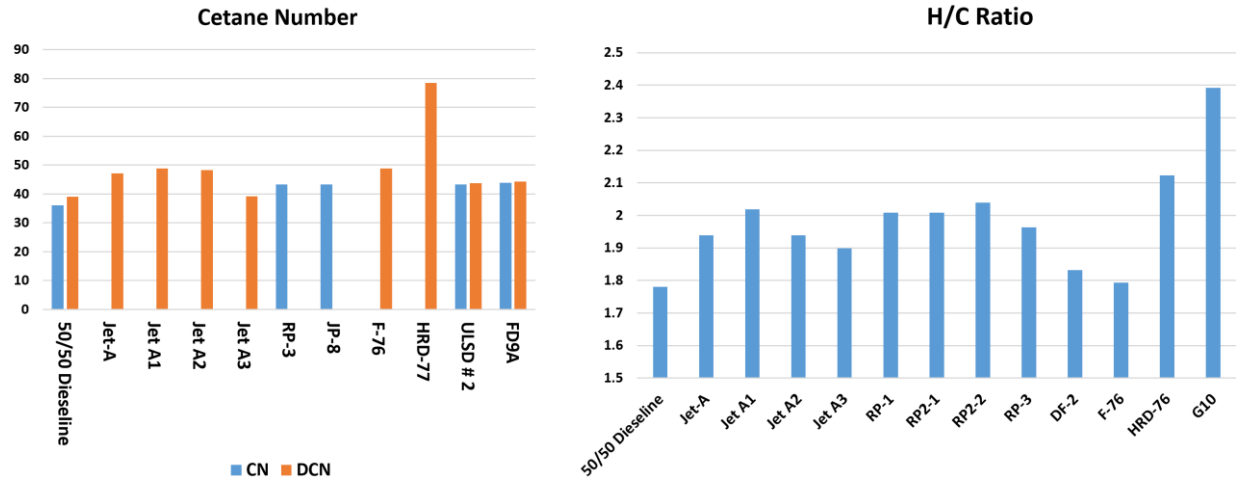

(a) (b)

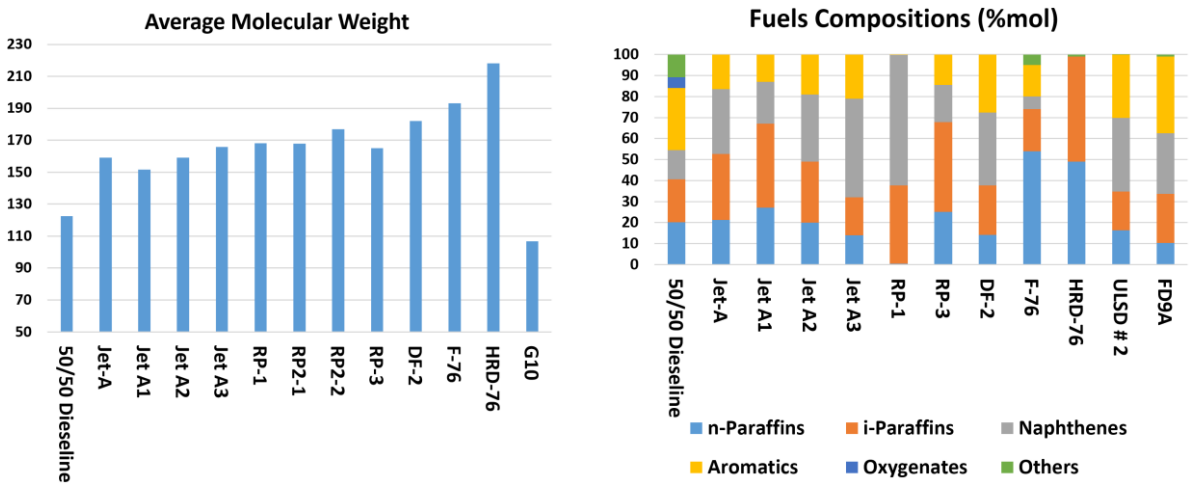

(c) (d)

Fig. 13. Fuel properties comparison for 50/50 dieseline with low vaper pressure fuel. Jet-A, RP-1 and DF-2 by Alturaifi et al. [38]; Jet-A and JP8 by Vasu et al. [33]; F-76 and HRD-76 by Gowdagiri et al. [41]; G10 by Davidson et al. [37] ; Jet-A1, Jet-A2 and Jet-A3 by Burden et al. [41]; RP-3 by Mao et al. [63]; Jet-A1, Jet-A2, Jet-A3, RP2-1 and RP2-2 by Davidson et al. [36]; FD9A and ULSD#2 by et al. [48].

In Fig. 14, the effect of cetane number on IDTs in the NTC region is investigated. Fuels shown in Fig. 14(a) have cetane number between 39.0 and 48.8. There is a clear effect of cetane number on the overall reactivity of the fuels in the NTC region. The fuels having a cetane number close to that of the 50/50 dieseline exhibit similar NTC reactivity. On the other hand, fuels with higher cetane numbers show increased reactivity. Similar behavior was observed by comparing the 50/50 dieseline with low-octane gasoline fuels in Fig. 11(a). At high temperatures, Fig. 14(a), the effect of cetane number on fuel reactivity is weaker. A comparison at 20 bar is provided in Fig. S4 (Supplementary materials). Figure 14(b) shows a comparison of IDTs measured in rapid compression machine. Again, the 50/50 dieseline blend has similar IDTs as FD9A and ULSD#2 which have DCN values not too far from the dieseline blend.

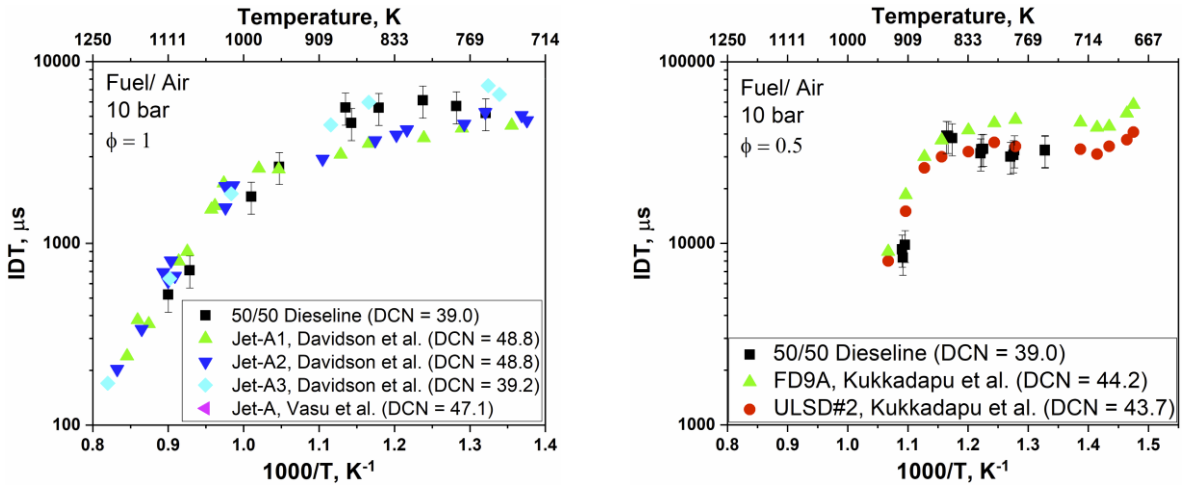

(a) (b)

Fig. 14. Effect of cetane number on IDTs. Jet-A by Vasu et al. [33]; RP-3 by Mao et al. [63]; Jet-A1, Jet-A2 and Jet-A3 by Davidson et al. [36]; FD9A and ULSD#2 by Kukkadapu et al. [48].

3.5.3. Mid-Octane Gasoline Like Fuels

The 25/75 dieseline blend is compared with different mid-octane gasoline fuels in Fig. 15. The fuels have RONs of between 77 and 84.7. All fuels exhibit very similar reactivities at high temperatures, Fig. 15(a), and in the NTC region, Fig. 15(b). The PRF 80 surrogate fuel shows slightly faster IDTs in the NTC and low temperatures, probably because PRF 80 only consists of paraffins and has zero octane sensitivity. It may be concluded from IDT and fuel property comparisons in Fig. 15 and 16 that gasoline fuels and gasoline-like dieseline blend with similar octane numbers have approximately similar reactivity at high temperatures and in the NTC region. At low temperatures, these fuels may exhibit some differences in their reactivity as other fuel properties such as composition play important role at lower temperatures.

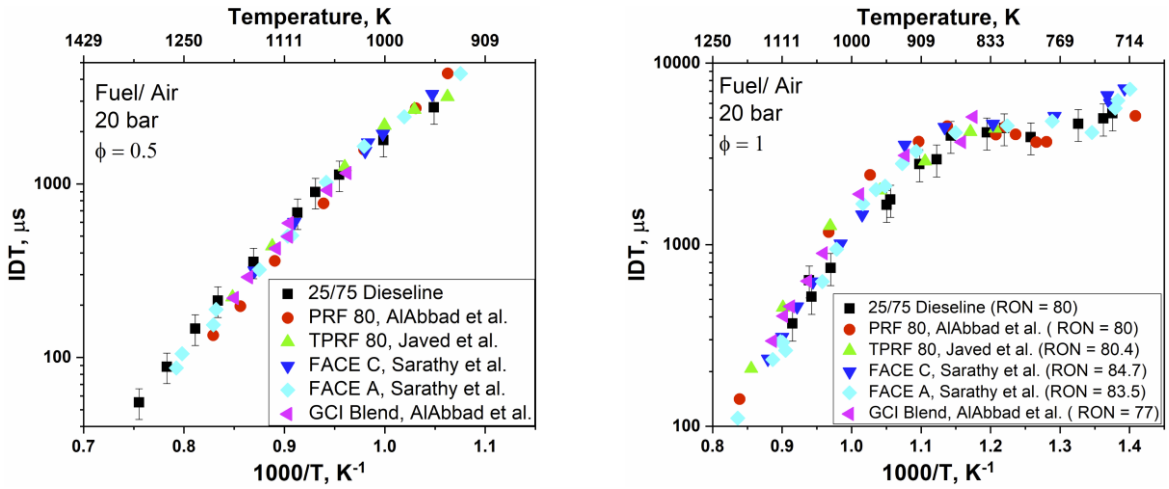

(a) (b)

Fig. 15. Comparison between 25/75 dieseline and mid-octane gasoline fuels. PRF 80 by AlAbbad et al. [52]; TPRF 80 by Javed et al. [64]; FACE A and C by Sarathy et al. [27]; GCI blend by AlAbbad et al. [31].

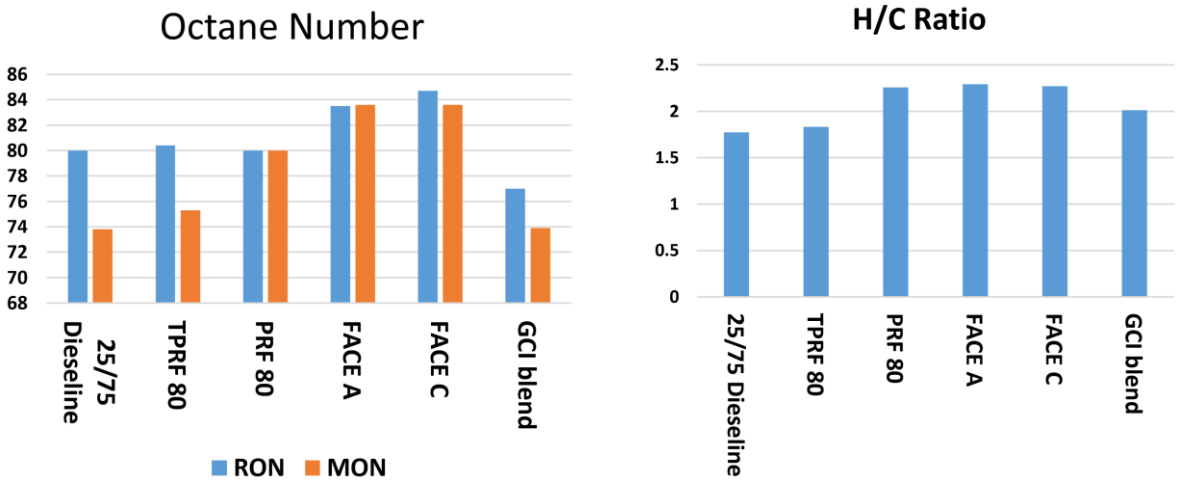

(a) (b)

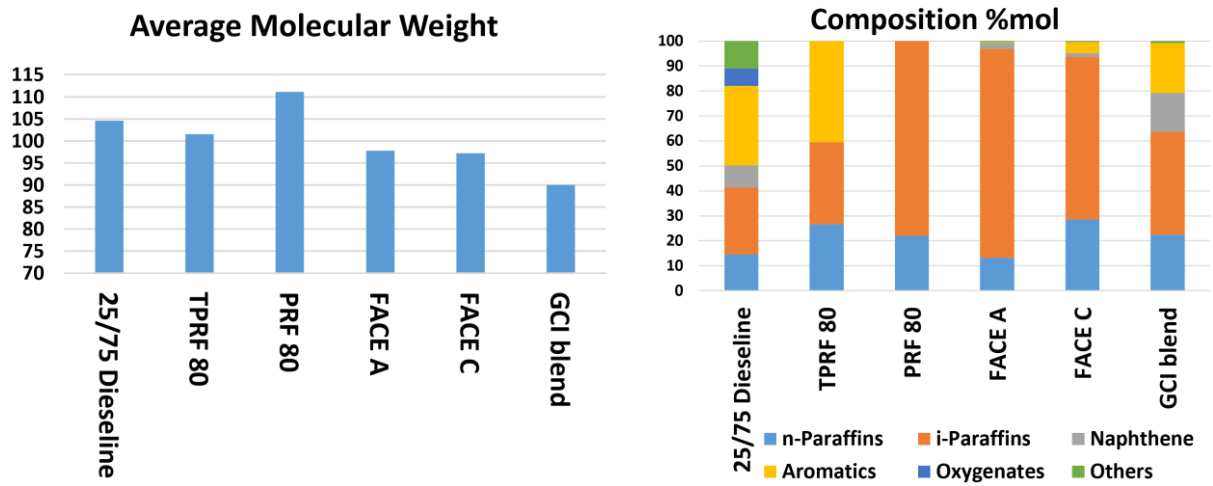

(c) (d)

Fig. 16. Fuel properties comparison for 25/75 dieseline with mid-octane gasoline. PRF 80 by AlAbbad et al. [52]; TPRF 80 by Javed et al. [64]; FACE A and C by Sarathy et al. [27]; GCI blend by AlAbbad et al. [31].

3.6. Comparison with Surrogates

Measured IDTs of the two dieseline blends are compared with the measured IDTs of the proposed multi-component surrogates (MCSs) and with simulated IDTs of PRF and TPRF surrogates. The PRF surrogate is formulated to match the RON of the target dieseline blend, while the TPRF surrogate is formulated to match both RON and MON of the target dieseline blend using the methodology proposed by Kalghatgi et a. [65]. The details concerning the MCS formulation are provided in Section 2.6. More details of the fuels and the surrogates are given in Table 8.

	50/50 Dieseline	**PRF 61**	**TPRF 61**	**50/50 MCS**	**25/75 Dieseline**	**PRF 80**	**TPRF 80**	**25/75 MCS**
RON	61	61	61	–	80	80	80	–
MON	55	61	55	–	73.8	80	73.8	–
n-Paraffins	20.2	41.92	45.82	15.7	14.5	22.01	27.16	12.7
i-Paraffins	20.4	58.08	11.54	25.3	26.8	77.99	28.76	27.5
Naphthenes	13.9	0	0	8.2	8.9	0	0	6.0
Aromatics	29.5	0	42.64	37	31.8	0	44.09	35.4
Oxygenates	5.2	0	0	6	6.9	0	0	7.9
Olefins	7.2	0	0	8	9.4	0	0	10.5

Indane & tetraline	3.6	0	0	0	1.6	0	0	0
Average MW	122.50	108.35	98.39	124.17	104.60	111.14	100.69	108.07
H/C	1.78	2.27	1.81	1.85	1.77	2.28	1.79	1.82

Table 8. Dieseline blends, PRF and TPRF surrogate properties. Compositions are given in mole%.

For PRF and TPRF surrogates, experimental IDT measurements were not carried out because the kinetic models are expected to do a reasonable job in predicting the reactivity of these simple surrogates. IDT simulations of PRF and TPRF surrogates were carried out with CHEMKIN-PRO [66] using the detailed iso-octane chemical kinetic model by Atef et al. [67]. The zero-D closed homogeneous batch reactor was used to emulate both shock tube and RCM conditions. To emulate the gradual pressure rise behind reflected shock wave, dp_5/dt (4.5% /ms) was converted to a volume history and imposed in the CHEMKIN-PRO simulations. To account for the facility effects in the RCM experiments, non-reactive pressure profiles were converted to volume profiles and imposed in the simulations. Figure 17(a) shows a comparison between the shock tube measured IDTs of the dieseline blends and the simulated IDTs of the corresponding PRF and TPRF surrogates. As expected, the TPRF surrogates (dashed lines) show lower reactivities compared to the PRF surrogates (solid lines) due to the low reactivity of toluene. At high temperatures, the surrogate simulations over-estimate the measured IDTs of the dieseline blends, with a larger deviation for the 50/50 dieseline. In the NTC region and low temperatures, the PRF surrogates do an overall good job of reproducing the reactivity of the dieseline blends. The comparisons illustrate that using a two-component PRF surrogate is sufficient to simulate the 25/75 dieseline blend over our experimental conditions for stoichiometric mixtures. For the 50/50 dieseline blend, however, PRF surrogate is able to reproduce the reactivity of the blend only in the NTC region and low temperatures.

Figure 17(b) show a comparison between the RCM IDT measurements and surrogate simulations for the 25/75 dieseline blend. As seen in Fig. 17(a), PRF surrogate does a good job of predicting the dieseline reactivity at ϕ = 1.0. However, both surrogates overestimate and underestimate the dieseline reactivity at ϕ = 2.0 and ϕ = 0.5, respectively. Further comparisons are provided in Fig. S5 (Supplementary Materials). These results illustrate that more complex surrogates may be needed to capture the reactivity of the dieseline blends over a wide range of conditions. Therefore, a multi-component surrogate (MCS) is proposed to overcome the limitations of PRF and TPRF surrogates.

In order to assess the adequacy of the MCSs in capturing the reactivity of the dieseline blends, IDTs of stoichiometric mixtures of the MCSs were measured at 20 bar and compared with the dieseline blends in Fig. 18. Overall, the measured IDTs of the dieseline blends and MCSs are in good agreement under our experimental conditions. Compared to PRF and TPRF surrogates, the MCSs provide improved performance.

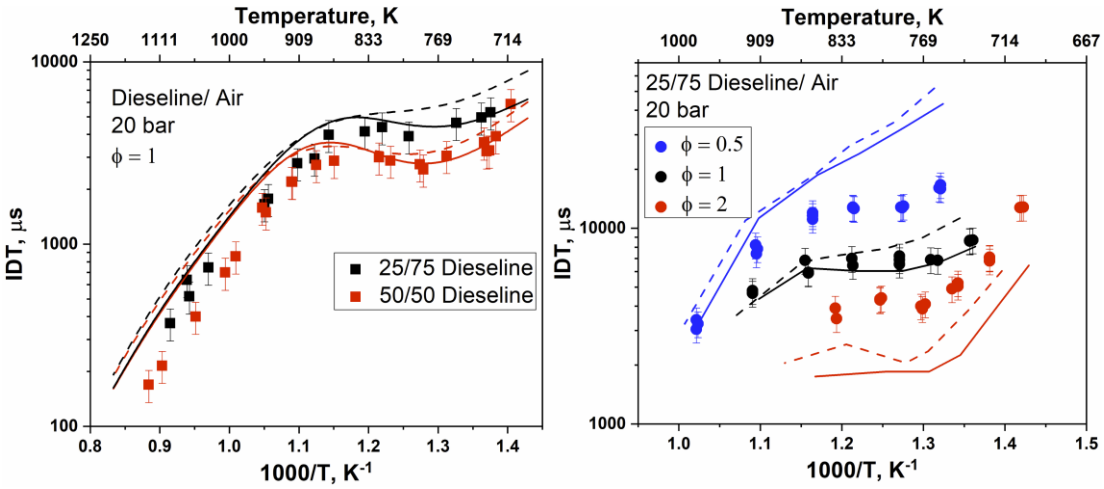

(a) (b)

Fig. 17. Comparison between measured IDTs of the dieseline blends and the simulations of surrogates. (a) Shock tube (b) RCM. Solid lines for PRF and dashed lines for TPRF (PRF 61 and TPRF 61 for dieseline 50/50; PRF 80 and TPRF 80 for dieseline 25/75).

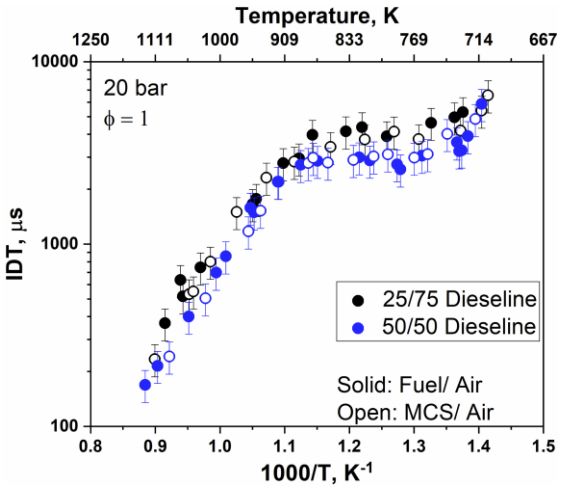

Fig. 18. Comparison between measured IDTs of dieseline blends and multi-component surrogates (MCSs).

4. Conclusions

IDTs of two dieseline blends (50/50 and 25/75 dieseline blends) were measured in shock tube and rapid compression machine. The blends had very low vapor pressures, and therefore the shock tube and the RCM facilities were heated. To ensure full evaporation and to avoid fuel condensation as well as decomposition or oxidation, NMR and laser absorption techniques were implemented to use optimal pre-heat temperatures. Comparing the measured IDTs of the dieseline blends at different pressures and equivalence ratios revealed that the effect of pressure and equivalence ratio on IDTs is strong in the NTC region and weak at high and low temperatures. The effect of the blending ratio of diesel and gasoline is also stronger in the NTC region. IDTs of the dieseline blends are also compared with previous experimental studies of low- and mid-octane gasoline fuels as well as low- and high-cetane fuels. The comparison revealed that gasoline fuels have lower reactivity at high temperatures compared to the dieseline blends. The 50/50 dieseline blend is much faster than the compared gasoline fuels. In the NTC region, fuels with similar octane numbers exhibit similar reactivity. Comparison of 50/50 dieseline and jet fuels / diesel shows that cetane number does not appear to have significant influence on IDTs at high temperatures though two diesel fuels exhibited slightly faster reactivity due to the presence of large hydrocarbons. Fuels with similar cetane numbers showed similar reactivities in the NTC region.

Simulated IDTs of two-component (PRF) and three-component (TPRF) surrogates are compared to the measured IDTs of the dieseline blends. For shock tube measurements, the PRF surrogate does a good job of emulating the reactivity of 25/75 dieseline from high to low temperatures. For the 50/50 dieseline, PRF surrogate matches fuel reactivity in the NTC region but it is slower at high temperatures. The TPRF surrogates do not provide improved performance compared to the PRF surrogates. For RCM measurements, the PRF surrogates predict the reactivity of the blends for stoichiometric mixtures but do a poor job at rich and lean conditions. This illustrates the need of developing a chemical kinetic model for multi-component surrogates to capture the reactivity of the dieseline blends over wide ranges of conditions.

Acknowledgements

The paper is based on work supported by Saudi Aramco Research and Development Center FUELCOM program under Master Research Agreement Number 6600024505/01 and the Office of Sponsored Research (OSR) at King Abdullah University of Science and Technology (KAUST). FUELCOM (Fuel Combustion for Advanced Engines) is a collaborative research undertaking between Saudi Aramco and KAUST intended to address the fundamental aspects of hydrocarbon fuel combustion in engines, and develop fuel/engine design tools suitable for advanced combustion modes. The authors at NUI Galway recognize funding support from Science Foundation Ireland (SFI) via their Principal Investigator Program through project number 15/IA/3177.

5. References

[1] Annual Energy Outlook 2019 with projection to 2050, Washington, US, 2019.
[2] J. Benajes, R. Novella, A. Garcia, V. Domenech, R. Durrett, An investigation on mixing and auto-ignition using diesel and gasoline in a direct-injection compression-ignition engine operating in PCCI combustion conditions, SAE International Journal of Engines 4 (2011) 2590-2602.
[3] F. Zhang, S.Z. Rezaei, H. Xu, S.-J. Shuai, Experimental investigation of different blends of diesel and gasoline (dieseline) in a CI engine, SAE International Journal of Engines 7 (2014) 1920-1930.
[4] S.Z. Rezaei, F. Zhang, H. Xu, A. Ghafourian, J.M. Herreros, S. Shuai, Investigation of two-stage split-injection strategies for a Dieseline fuelled PPCI engine, Fuel 107 (2013) 299-308.
[5] S. Zeraati-Rezaei, Y. Al-Qahtani, H. Xu, Investigation of hot-EGR and low pressure injection strategy for a Dieseline fuelled PCI engine, Fuel 207 (2017) 165-178.
[6] G. Kalghatgi, Fuel Effects on Autoignition in Premixed Systems—Knock in Spark Ignition Engines and Combustion in Homogeneous Charge Compression Ignition Engines, SAE2014.
[7] Y. Viollet, J. Chang, G. Kalghatgi, Compression ratio and derived cetane number effects on gasoline compression ignition engine running with naphtha fuels, SAE International Journal of Fuels and Lubricants 7 (2014) 412-426.
[8] G.T. Kalghatgi, The outlook for fuels for internal combustion engines, International Journal of Engine Research 15 (2014) 383-398.
[9] G. Kalghatgi, B. Johansson, Gasoline compression ignition approach to efficient, clean and affordable future engines, Proceedings of the Institution of Mechanical Engineers, Part D: Journal of Automobile Engineering 232 (2018) 118-138.
[10] G. Kalghatgi, L. Hildingsson, B. Johansson, Low NOx and low smoke operation of a diesel engine using gasolinelike fuels, Journal of engineering for gas turbines and power 132 (2010) 092803.
[11] M.P. Musculus, P.C. Miles, L.M. Pickett, Conceptual models for partially premixed low-temperature diesel combustion, Progress in energy and combustion science 39 (2013) 246-283.
[12] D. Turner, G. Tian, H. Xu, M.L. Wyszynski, E. Theodoridis, An experimental study of dieseline combustion in a direct injection engine, Report No. 0148-7191, SAE Technical Paper, 2009.
[13] A. Weall, N. Collings, Investigation into partially premixed combustion in a light-duty multi-cylinder diesel engine fuelled with a mixture of gasoline and diesel, Report No. 0148-7191, SAE Technical Paper, 2007.
[14] H.W. Won, H. Pitsch, N. Tait, G. Kalghatgi, Some effects of gasoline and diesel mixtures on partially premixed combustion and comparison with the practical fuels gasoline and diesel in a compression ignition engine, Proceedings of the Institution of Mechanical Engineers, Part D: Journal of Automobile Engineering 226 (2012) 1259-1270.
[15] X. Lu, Y. Qian, Z. Yang, D. Han, J. Ji, X. Zhou, Z. Huang, Experimental study on compound HCCI (homogenous charge compression ignition) combustion fueled with gasoline and diesel blends, Energy 64 (2014) 707-718.
[16] D. Han, A.M. Ickes, D.N. Assanis, Z. Huang, S.V. Bohac, Attainment and load extension of high-efficiency premixed low-temperature combustion with dieseline in a compression ignition engine, Energy & Fuels 24 (2010) 3517-3525.
[17] F. Zhang, H. Xu, S.Z. Rezaei, G. Kalghatgi, S.-J. Shuai, Combustion and emission characteristics of a PPCI engine fuelled with dieseline, Report No. 0148-7191, SAE Technical Paper, 2012.
[18] S. Zeraati-Rezaei, Y. Al-Qahtani, J.M. Herreros, X. Ma, H. Xu, Experimental investigation of particle emissions from a Dieseline fuelled compression ignition engine, Fuel 251 (2019) 175-186.

[19] R. Vallinayagam, Y. An, S. Vedharaj, J. Sim, J. Chang, B. Johansson, Naphtha vs. dieseline–The effect of fuel properties on combustion homogeneity in transition from CI combustion towards HCCI, Fuel 224 (2018) 451-460.
[20] I.M. Algunaibet, A.K. Voice, G.T. Kalghatgi, H. Babiker, Flammability and volatility attributes of binary mixtures of some practical multi-component fuels, Fuel 172 (2016) 273-283.
[21] F. Zhang, H. Xu, J. Zhang, G. Tian, G. Kalghatgi, Investigation into light duty dieseline fuelled partially-premixed compression ignition engine, SAE International Journal of Engines 4 (2011) 2124-2134.
[22] J. Wang, Z. Wang, H. Liu, Combustion and emission characteristics of direct injection compression ignition engine fueled with Full Distillation Fuel (FDF), Fuel 140 (2015) 561-567.
[23] H. Liu, Z. Wang, J. Wang, X. He, Effects of gasoline research octane number on premixed low-temperature combustion of wide distillation fuel by gasoline/diesel blend, Fuel 134 (2014) 381-388.
[24] J. Wang, F. Yang, M. Ouyang, Dieseline fueled flexible fuel compression ignition engine control based on in-cylinder pressure sensor, Applied energy 159 (2015) 87-96.
[25] F. Yang, C. Yao, J. Wang, M. Ouyang, Load expansion of a dieseline compression ignition engine with multi-mode combustion, Fuel 171 (2016) 5-17.
[26] D. Jing, F. Zhang, Y. Li, H. Xu, S. Shuai, Experimental investigation on the macroscopic and microscopic spray characteristics of dieseline fuel, Fuel 199 (2017) 478-487.
[27] S.M. Sarathy, G. Kukkadapu, M. Mehl, W. Wang, T. Javed, S. Park, M.A. Oehlschlaeger, A. Farooq, W.J. Pitz, C.-J. Sung, Ignition of alkane-rich FACE gasoline fuels and their surrogate mixtures, Proceedings of the Combustion Institute 35 (2015) 249-257.
[28] T. Javed, A. Ahmed, L. Lovisotto, G. Issayev, J. Badra, S.M. Sarathy, A. Farooq, Ignition studies of two low-octane gasolines, Combustion and Flame 185 (2017) 152-159.
[29] S.M. Sarathy, A. Farooq, G.T. Kalghatgi, Recent progress in gasoline surrogate fuels, Progress in Energy and Combustion Science 65 (2018) 67-108.
[30] M. Alabbad, G. Issayev, J. Badra, A.K. Voice, B.R. Giri, K. Djebbi, A. Ahmed, S.M. Sarathy, A. Farooq, Autoignition of straight-run naphtha: A promising fuel for advanced compression ignition engines, Combustion and Flame 189 (2018) 337-346.
[31] M. AlAbbad, J. Badra, K. Djebbi, A. Farooq, Ignition delay measurements of a low-octane gasoline blend, designed for gasoline compression ignition (GCI) engines, Proceedings of the Combustion Institute 37 (2019) 171-178.
[32] C. Lee, A. Ahmed, E.F. Nasir, J. Badra, G. Kalghatgi, S.M. Sarathy, H. Curran, A. Farooq, Autoignition characteristics of oxygenated gasolines, Combustion and Flame 186 (2017) 114-128.
[33] S.S. Vasu, D.F. Davidson, R.K. Hanson, Jet fuel ignition delay times: Shock tube experiments over wide conditions and surrogate model predictions, Combustion and flame 152 (2008) 125-143.
[34] G. Flora, J. Balagurunathan, S. Saxena, J.P. Cain, M.S. Kahandawala, M.J. DeWitt, S.S. Sidhu, E. Corporan, Chemical ignition delay of candidate drop-in replacement jet fuels under fuel-lean conditions: A shock tube study, Fuel 209 (2017) 457-472.
[35] D.J. Valco, K. Min, A. Oldani, T. Edwards, T. Lee, Low temperature autoignition of conventional jet fuels and surrogate jet fuels with targeted properties in a rapid compression machine, Proceedings of the Combustion Institute 36 (2017) 3687-3694.
[36]

D.F. Davidson, Y. Zhu, S. Wang, T. Parise, R. Sur, R.K. Hanson. Shock Tube Measurements of Jet and Rocket Fuels. In: editor^editors. 54th AIAA Aerospace Sciences Meeting; 2016. p. 0178.
[37] D. Davidson, Y. Zhu, J. Shao, R. Hanson, Ignition delay time correlations for distillate fuels, Fuel 187 (2017) 26-32.
[38] S.A. Alturaifi, R.L. Rebagay, O. Mathieu, B. Guo, E.L. Petersen, A Shock-Tube Autoignition Study of Jet, Rocket, and Diesel Fuels, Energy & fuels 33 (2019) 2516-2525.

[39]

Y. Wang, Y. Cao, D.F. Davidson, R.K. Hanson. Ignition delay time measurements for distillate and synthetic jet fuels. In: editor^editors. AIAA Scitech 2019 Forum; 2019. p. 2248.
[40] D.R. Haylett, D.F. Davidson, R.K. Hanson, Ignition delay times of low-vapor-pressure fuels measured using an aerosol shock tube, Combustion and Flame 159 (2012) 552-561.
[41] S. Gowdagiri, W. Wang, M.A. Oehlschlaeger, A shock tube ignition delay study of conventional diesel fuel and hydroprocessed renewable diesel fuel from algal oil, Fuel 128 (2014) 21-29.
[42] L. Yu, S. Wang, W. Wang, Y. Qiu, Y. Qian, Y. Mao, X. Lu, Exploration of chemical composition effects on the autoignition of two commercial diesels: Rapid compression machine experiments and model simulation, Combustion and Flame 204 (2019) 204-219.
[43] S. Wang, L. Yu, Z. Wu, Y. Mao, H. Li, Y. Qian, L. Zhu, X. Lu, Gas-phase autoignition of diesel/gasoline blends over wide temperature and pressure in heated shock tube and rapid compression machine, Combustion and Flame 201 (2019) 264-275.
[44] S. Wang, Y. Feng, Y. Qian, Y. Mao, M. Raza, L. Yu, X. Lu, Experimental and kinetic study of diesel/gasoline surrogate blends over wide temperature and pressure, Combustion and Flame 213 (2020) 369-381.
[45] D. Haylett, P. Lappas, D. Davidson, R. Hanson, Application of an aerosol shock tube to the measurement of diesel ignition delay times, Proceedings of the Combustion Institute 32 (2009) 477-484.
[46] K. Kumar, C.-J. Sung, An experimental study of the autoignition characteristics of conventional jet fuel/oxidizer mixtures: Jet-A and JP-8, Combustion and Flame 157 (2010) 676-685.
[47] V.N. Hoang, L.D. Thi, Experimental study of the ignition delay of diesel/biodiesel blends using a shock tube, Biosystems Engineering 134 (2015) 1-7.
[48] G. Kukkadapu, C.-J. Sung, Autoignition study of ULSD# 2 and FD9A diesel blends, Combustion and Flame 166 (2016) 45-54.
[49] S. Burden, A. Tekawade, M.A. Oehlschlaeger, Ignition delay times for jet and diesel fuels: Constant volume spray and gas-phase shock tube measurements, Fuel 219 (2018) 312-319.
[50] L. Yu, Y. Mao, Y. Qiu, S. Wang, H. Li, W. Tao, Y. Qian, X. Lu, Experimental and modeling study of the autoignition characteristics of commercial diesel under engine-relevant conditions, Proceedings of the Combustion Institute 37 (2019) 4805-4812.
[51] T. Javed, E.F. Nasir, A. Ahmed, J. Badra, K. Djebbi, M. Beshir, W. Ji, S.M. Sarathy, A. Farooq, Ignition delay measurements of light naphtha: A fully blended low octane fuel, Proceedings of the Combustion Institute 36 (2017) 315-322.
[52] M. AlAbbad, T. Javed, F. Khaled, J. Badra, A. Farooq, Ignition delay time measurements of primary reference fuel blends, Combustion and Flame 178 (2017) 205-216.
[53] K. Zhang, C. Banyon, C. Togbé, P. Dagaut, J. Bugler, H.J. Curran, An experimental and kinetic modeling study of n-hexane oxidation, Combustion and Flame 162 (2015) 4194-4207.
[54] L. Brett, J. Macnamara, P. Musch, J.M. Simmie, Simulation of methane autoignition in a rapid compression machine with creviced pistons, Combustion and Flame 124 (2001) 326-329.
[55] A.G. Abdul Jameel, V. Van Oudenhoven, A.-H. Emwas, S.M. Sarathy, Predicting octane number using nuclear magnetic resonance spectroscopy and artificial neural networks, Energy & fuels 32 (2018) 6309-6329.
[56] A. Sarpal, G. Kapur, S. Mukherjee, A. Tiwari, PONA analyses of cracked gasoline by 1H NMR spectroscopy. Part II, Fuel 80 (2001) 521-528.
[57] B. Basu, G. Kapur, A. Sarpal, R. Meusinger, A neural network approach to the prediction of cetane number of diesel fuels using nuclear magnetic resonance (NMR) spectroscopy, Energy & fuels 17 (2003) 1570-1575.

[58] A.G. Abdul Jameel, N. Naser, A.-H. Emwas, S. Dooley, S.M. Sarathy, Predicting fuel ignition quality using 1H NMR spectroscopy and multiple linear regression, Energy & Fuels 30 (2016) 9819-9835.
[59] A.G. Abdul Jameel, N. Naser, A.-H. Emwas, S.M. Sarathy, Surrogate formulation for diesel and jet fuels using the minimalist functional group (MFG) approach, Proceedings of the Combustion Institute 37 (2019) 4663-4671.
[60] M.D. Boot, M. Tian, E.J. Hensen, S.M. Sarathy, Impact of fuel molecular structure on auto-ignition behavior–Design rules for future high performance gasolines, Progress in Energy and Combustion Science 60 (2017) 1-25.
[61] D. Valco, G. Gentz, C. Allen, M. Colket, T. Edwards, S. Gowdagiri, M.A. Oehlschlaeger, E. Toulson, T. Lee, Autoignition behavior of synthetic alternative jet fuels: An examination of chemical composition effects on ignition delays at low to intermediate temperatures, Proceedings of the Combustion Institute 35 (2015) 2983-2991.
[62] J.C. Andrae, Development of a detailed kinetic model for gasoline surrogate fuels, Fuel 87 (2008) 2013-2022.
[63] Y. Mao, L. Yu, Z. Wu, W. Tao, S. Wang, C. Ruan, L. Zhu, X. Lu, Experimental and kinetic modeling study of ignition characteristics of RP-3 kerosene over low-to-high temperature ranges in a heated rapid compression machine and a heated shock tube, Combustion and Flame 203 (2019) 157-169.
[64] T. Javed, C. Lee, M. AlAbbad, K. Djebbi, M. Beshir, J. Badra, H. Curran, A. Farooq, Ignition studies of n-heptane/iso-octane/toluene blends, Combustion and Flame 171 (2016) 223-233.
[65] G. Kalghatgi, H. Babiker, J. Badra, A simple method to predict knock using toluene, n-heptane and iso-octane blends (TPRF) as gasoline surrogates, SAE International Journal of Engines 8 (2015) 505-519.
[66] R. CHEMKIN-PRO, 15112, Reaction Design, Inc., San Diego, CA, (2011).
[67] N. Atef, G. Kukkadapu, S.Y. Mohamed, M. Al Rashidi, C. Banyon, M. Mehl, K.A. Heufer, E.F. Nasir, A. Alfazazi, A.K. Das, A comprehensive iso-octane combustion model with improved thermochemistry and chemical kinetics, Combustion and Flame 178 (2017) 111-134.